ACS Sustainable Chemistry & Engineering

Research Article

pubs.acs.org/journal/ascecg

Employing Easily Prepared Carbon Nanoparticles To Improve Performance of Inverted Organic Solar Cells

Xinyuan Zhang,[†] Zhiqi Li,[†] Zhihui Zhang,[†] Chunyu Liu,[†] Jinfeng Li,[†] Wenbin Guo,*[,†] and Songnan Qu*[,‡]

[†]State Key Laboratory on Integrated Optoelectronics, College of Electronic Science and Engineering, Jilin University, 2699 Qianjin Street, Changchun 130012, China

[‡]State Key Laboratory of Luminescence and Applications, Changchun Institute of Optics, Fine Mechanics and Physics, Chinese Academy of Sciences, 3888 Eastern South Lake Road, Changchun130033, China

ABSTRACT: In this paper, we demonstrate that the efficiency of P3HT:ICBA blend -based organic solar cells (OSCs) was dramatically enhanced by introducing carbon nanoparticles (CNPs) into the active layer. At the optimal doping concentration, the power conversion efficiency (PCE) of doped devices was increased from 4.12% up to 5.90%, accounting for a 43.20% PCE enhancement. CNPs serve as scattering centers to enlarge the light pathways, resulting in light-harvesting improvements. Meanwhile, the incorporation of CNPs in P3HT:ICBA blend can form a perfect homogeneous interpenetrating network, which is beneficial to improve exciton dissociation, charge transport, charge collection, and the photoconductive property of solar cells. This study establishes an efficient method for fabricating high-performance OSCs based on commercially available donor and acceptor materials.

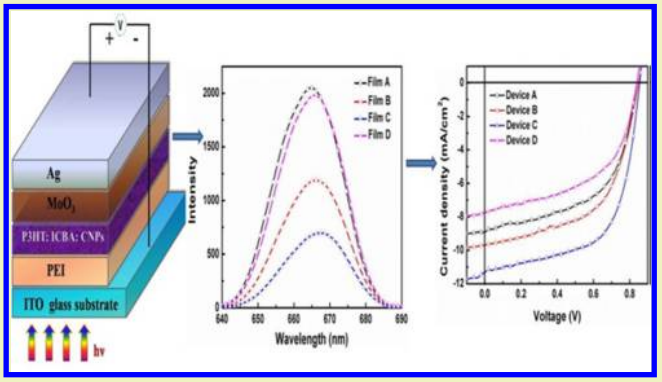

KEYWORDS: *Light absorption, Exciton generation, Exciton dissociation, Charge transport, Mobility, Impedance, Charge collection*

INTRODUCTION

Excessive consumption of fossil fuel has brought a series of issues to society's progress, such as haze, energy crisis, and the ecological damage.[1−3] Solution-processed bulk heterojunction (BHJ) organic solar cells (OSCs) based on conjugated polymer:fullerene composites have received considerable attention as one of the promising alternatives for environment-friendly and renewable energy source with the merits of cost-effective fabrication, light weight, mechanical flexibility, and the abundance of the organic materials.[4−8] Intensive research has been conducted toward the development of OSCs based on BHJ concept such as designing novel device structures and material innovations (e.g., frontier donor/acceptor materials), and dramatically improved power conversion efficiency (PCE) from 3% to almost 10%.[9−11] The highest reported open-circuit voltage (V_{oc}) for the prevalent poly(3-hexylthiophene) (P3HT):[6,6]-phenyl-C_{61}-butyric acid methyl ester (PCBM) cells is around 0.66 V, which limits device efficiency development. In attempt to find novel electron-accept polymers, more recently indene−C_{60} bisadduct (ICBA), when blended with P3HT, has achieved a higher open-circuit voltage (0.84 V) than PCBM due to its smaller electron affinity, resulting in enhanced device efficiency.[12]

Despite the encouraging achievements that have been made during past decades, OSCs still offer a large room for performance improvement to achieve commercial applications. The development of higher PCEs has heavily relied on the fate of photocharge carriers after exciton dissociation, which is primarily ruled by the trade-off between charge extraction at interface, charge recombination, and their collection efficiency at the respective electrodes.[13,14] Due to the lack of valid pathways for each type of carrier, enhancing the light absorption by the active layer does not mean that there is a realistic increase of free carriers; the BHJ structure is often considered less optimal for charge transport.[15] Many different efforts have been exploited to address this challenge, e.g., interface/morphology engineering to utilize the full potential of OSCs.[16−21] Incorporating nanomaterials, such as nanoparticles (NPs), nanorods (NRs), or nanotubes (NTs), within the active layer is one of the most straightforward and practical ways to achieve the ideal BHJ morphology, forming a perfect homogeneous interpenetrating network, leading to the improvement of the overall charge splitting and migration.[22−26]

In this respect, carbon NPs (CNPs) are an ideal additive because of their excellent electrical conduction, manufactured elasticity, and compatibility with the solution process, without the need for any vacuum systems or etching processes, thereby saving time and money.[27,28] Furthermore, the NPs can act as a scattering center or an energy transfer agent, and the optical path within the active layer lengthens through the forward

Received: January 6, 2016
Revised: February 17, 2016
Published: February 22, 2016

DOI: 10.1021/acssuschemeng.6b00036
ACS Sustainable Chem. Eng. 2016, 4, 2359−2365

scattering from NPs, thereby enhancing the probability of light absorption.[29−34]

In this contribution, we present synergistic enhancements of excition generation, charge dissociation, and charge transport property of OSCs by incorporating new synthetic CNPs. We introduced the CNPs as an additive into a host system of P3HT/ICBA blend, and various concentrations were selected to optimize the performance of cells. As a result, the short-circuit current (J_{sc}) and fill factor (FF) were simultaneously improved, and PCE of 5.90% was achieved upon optimizing the amount of CNPs in single BHJ cells with an inverted device structure. The motivation of this work was to investigate CNPs' reaction mechanism including the trimming of morphology, influence on exciton dissociation, and charge transportation, therefore, unraveling the feasibility of using CNPs as the additive in the optimization of OSCs.

EXPERIMENTAL SECTION

Carbon Nanoparticles' Preparation and Property. The microwave synthesis of CNPs follows procedures that were given in our previous work.[35,36] Citric acid (3 g) and urea (6 g) were added to distilled water (20 mL) to form a transparent solution. The solution was then heated in a domestic 650 W microwave oven for 4−5 min, during which the solution changed from a colorless liquid, to a brown liquid, and finally a dark-brown clustered solid, indicating the formation of CNPs. This solid was then transferred to a vacuum oven and heated at 60 °C for 1 h. A sample of the CNPs was diluted in aqueous solution, which was purified in a centrifuge (10000 rpm, 20 min) to remove large or agglomerated particles.

The morphologies of CNPs were characterized using transmission electron microscopy (TEM). Drops of the dilute aqueous solution of CNPs were deposited on carbon-coated copper grids for TEM. Morphology characterizations illustrate that CNPs are spherical and well dispersed (Figure 1). The sizes of CNPs were in the range from 1

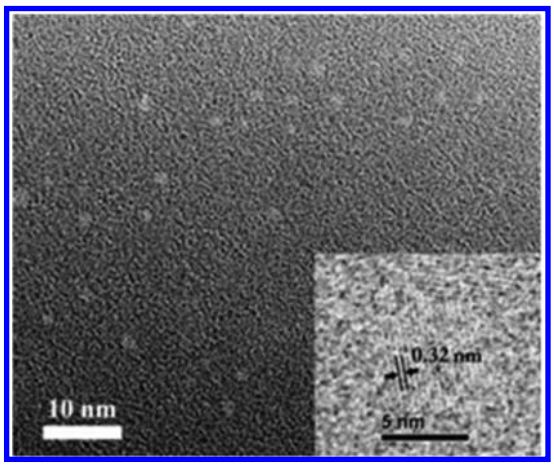

Figure 1. TEM morphology of CNPs.

to 5 nm. Well-resolved lattice fringes with an interplanar spacing of 0.32 nm of CNPs are close to the (002) facet of graphitic carbon.

Device Fabrication and Characterization. The device structure and energy levels of materials used in our study are shown in Figure 2, and the detailed configuration is glass/indium tin oxide (ITO) (150 nm)/amine-rich polymer (poly(ethylene imine)) (PEI) (25 nm)/P3HT:ICBA:CNPs (100 nm)/molybdenum oxide (MoO_3) (10 nm)/Ag (100 nm). ITO glass substrates were cleaned consecutively in ultrasonic baths containing acetone, detergent, deionized water, and ethanol and then dried by high purity nitrogen gas. In order to further clean the substrates and increase the work function of the ITO substrates, the precleaned substrates were treated with UV-ozone for 10 min. PEI applied as a hole-blocking layer was spin-coated at 4000 rpm on top of the ITO in air, then heated to 100 °C, and kept in glovebox for 10 min. We chose three doping amounts of 0.6, 0.9, and 1.2 mg CNPs in every milliliter blend 1,2-dichlorobenzene (DCB) solution composed of P3HT and ICBA forming the active layer of OSCs to optimize the devices performance. The corresponding weight ratios (wt) of CNPs and P3HT:ICBA blend are 2, 3, and 4 wt%, and the completely fabricated devices of pristine film and with 2, 3, and 4 wt% of CNPs are named Device A, Device B, Device C, and Device D, respectively. The blended P3HT:ICBA solutions without and with CNPs were spin-cast at 1500 rpm on top of the PEI layer and then thermal annealed in the glovebox at 150 °C for 25 min as active layer. Subsequently, the devices were completed by thermal evaporation of MoO_3 and Ag electrodes.[37−39] The absorption and reflectance spectra were measured by means of ultraviolet/visible spectrometer (UV1700, Shimadzu). Current density−voltage (J−V) characteristics of the finished devices were measured using a computer-programmed Keithley 2400 source/meter under AM1.5G solar illuminations with an Oriel 300 W solar simulator intensity of ∼100 mW cm^{-2} (about one sun) in air without encapsulation. The light intensity was measured with a photometer (International Light, IL1400) corrected by a standard silicon solar cell. The incident photon-to-current efficiency (IPCE) was measured with the Crowntech QTest Station 1000 AD instrument. The impedance was analyzed by a Wayne Kerr Electronics 6500B series precision impedance analyzer.

RESULTS AND DISCUSSION

Nanoscale additives, such as CNPs, may profoundly influence the morphology of the BHJ layer, which plays a crucial role in the device performance of OSCs.[40,41] As an initial study, we investigated the function of CNPs dopants on the morphological properties of the photoactive layer. Figure 3 show images of P3HT:ICBA films without and with the CNPs additive (2, 3, and 4 wt%, respectively) measured by atomic force microscopy (AFM). For pristine P3HT:ICBA layer (Figure 3a), the film exhibits a featureless and rough morphology; the corresponding root-mean-square (rms) is 3.68 nm. However, the film with 3 wt% CNPs (Figure 3c) possesses uniform and finer phase separation in the blend with a rms of 0.67 nm. The CNPs with small sizes (1.0−5.0 nm) can fill the gaps between P3HT and ICBA, and the active layer film with 2 wt% CNPs indicates a rms of 1.57 nm (Figure 3b). Such an interpenetrating network in the active layer could facilitate the formation of efficient exciton dissociation interfaces and form efficient percolation paths, assisting charge separation and minimizing bulk recombination. When the doping amount reaches 4 wt% (Figure 3d), the film becomes substantially uneven due to the aggregation of CNPs and the rms is 1.73 nm, forming large clusters. The net result is to destroy the interpenetrating pathway for charge transport, and the tough terrain may ruin the contact interfaces between layers, resulting in a poor performance especially for FF.

Figure 4a presents J−V characteristics of all fabricated devices and the values are typical averages of 40 devices. Simultaneously, detailed parameters, such as short-circuit current (J_{sc}), open-circuit voltage (V_{oc}), fill factor (FF), PCE, series resistance (R_s), and shunt resistance (R_{sh}), of devices without and with CNPs are summarized in Table 1. Device A, without any additive, shows a J_{sc} of 8.93 mA/cm^2, a V_{oc} of 0.84 V, and a FF of 54.92%, leading to a PCE of 4.12%. With the increase of CNPs doping concentration, PCEs of the doped devices show a tendency to first increase and then decrease, reaching the maximum of 5.90% at the optimal doping rate of 3 wt%, following with a J_{sc} of 11.31 mA/cm^2, a V_{oc} of 0.85 V, and a FF of 61.09%. Compared to the control device, the higher efficiency of Device C is mainly attributed to the increase of

DOI: 10.1021/acssuschemeng.6b00036
ACS Sustainable Chem. Eng. 2016, 4, 2359−2365

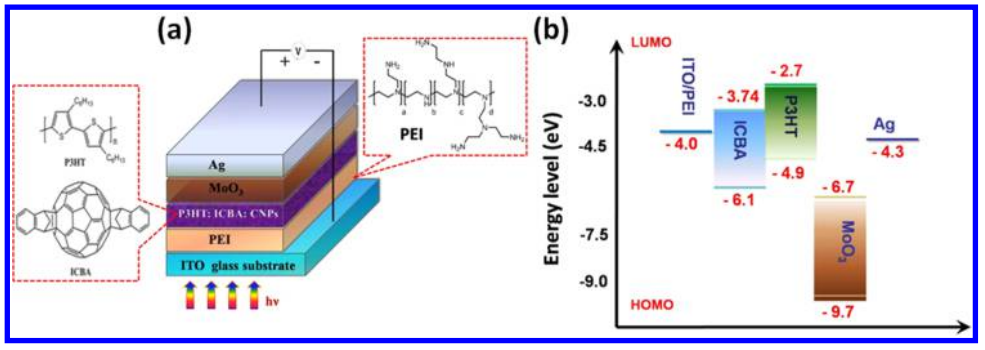

Figure 2. (a) Device structure and chemical structure of materials involved in this study. (b) Scheme of energy levels of the inverted organic solar cells.

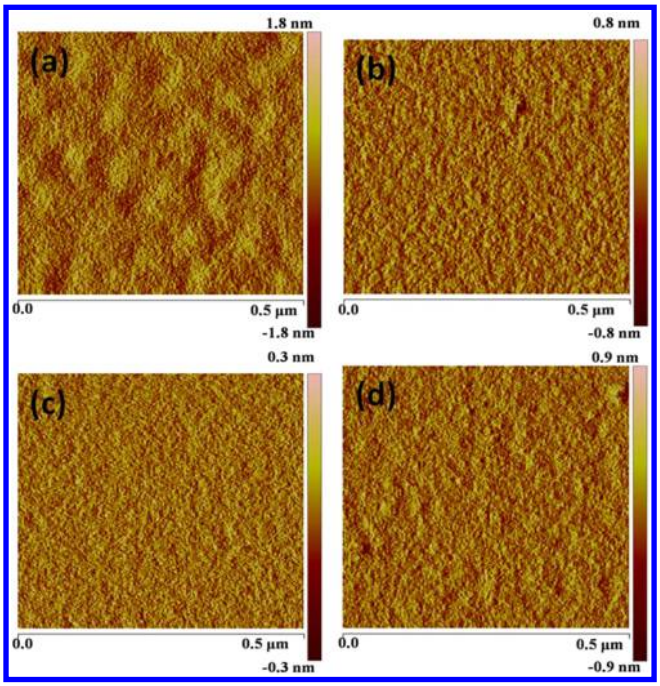

Figure 3. AFM morphology image of active layer films without and with CNPs: (a) pristine P3HT:ICBA film, and P3HT:ICBA layers doped with (b) 2 wt%, (c) 3 wt%, and (d) 4 wt% CNPs.

J_{sc} and FF, which own 26.74% and 11.23% enhancement, respectively, resulting in a remarkable improvement of PCE from 4.12% up to 5.90%. Ascribed to the moderate doping CNPs into active layer, an ideal donor−acceptor internetwork was obtained; thus, the charge carrier transport capability was enhanced and charge carriers recombination was reduced in the transport process, resulting in the significant improvement of J_{sc} and FF. The R_s and R_{sh} could be calculated according to the J−V curves:[42]

$$R_s = -(dV/dJ)_{V=V_{oc}} \quad (1)$$

and

$$R_{sh} = -(dV/dJ)_{J=J_{sc}} \quad (2)$$

The change trend of R_s first decreased and then showed a slight rebound with the increased doping amount of CNPs. The R_{sh} shows a remarkable increase first and then decreases with CNPs doping concentration. With the increase of doping amount of CNPs, the charge carrier mobility first enhanced and then reduced. After an optimal concentration of CNPs was doped, the interfaces of the active layer and the buffer layer could contact more closely, which is beneficial to free charge carriers extraction and injection to respective electrodes. Consequently, the R_s distinguishably decreased while the R_{sh} remarkably increased with CNPs doping, especially for Device C.[43] However, when more CNPs were added (over 3 wt%), the performance of Device D was deteriorated, which means that excess doping did damage to the nanoscale interpenetrating network and led to an inferior charge transport property.

Figure 4b shows the IPCE spectra of the OSCs with various CNPs doping concentrations; as expected, the IPCE data of Device C, with 3 wt% CNPs doping concentration, are the highest among all devices, which is in accordance with the observed performance from J−V characteristics. The IPCE spectrum of the doped cells was conspicuously improved in the region of 500−610 nm by doping appropriate amounts of CNPs. However, the IPCE spectra of the doped device significantly decreased from 400 to 510 nm when the CNPs doping amount increased to 4 wt%. A superfluous doping of additive in the active layers deteriorated the crystallization of the film and resulted in a negative impact on charge transport and collection, leading to the distinct decrease for J_{sc} and FF and, thus, indicating poor performance.

To investigate the effect of CNPs doping on the photon harvesting of active layer, the normalized UV−vis absorption spectra of the blend films were measured and are shown in Figure 4c, and the light-harvesting trend of active layer films is consistent with J−V curves. It can also be seen that the P3HT:ICBA:CNPs composite films have almost the same absorption range and the same peak position with that of undoped film. The doped film with appropriate doping amounts shows a significant absorption improvement in the region of 300−720 nm. The CNPs could act as scattering centers to increase the light path length in the active layer so that more photons can be trapped, which effectively contributes to the increase of J_{sc} and PCE.[44−47] However, the absorption intensity of the blend films distinctly decreases when the doping concentration reaches 4 wt%, which may be due to the distorted P3HT molecular arrangement induced by doping with excess CNPs and resulted in an adverse effect on light trapping of P3HT:ICBA. Thus, the donor/acceptor interface area and efficient pathways for the transportation of free charge carriers are impaired by the over-doped additive aggregation, which has negative impact on absorption as well as charge transportation, leading to a decreased J_{sc} and FF. Figure 4d demonstrates the variation tendency of active layer films reflections, which are fairly consistent with absorption spectra. These results are also in good agreement with the IPCE spectra

DOI: 10.1021/acssuschemeng.6b00036
ACS Sustainable Chem. Eng. 2016, 4, 2359−2365

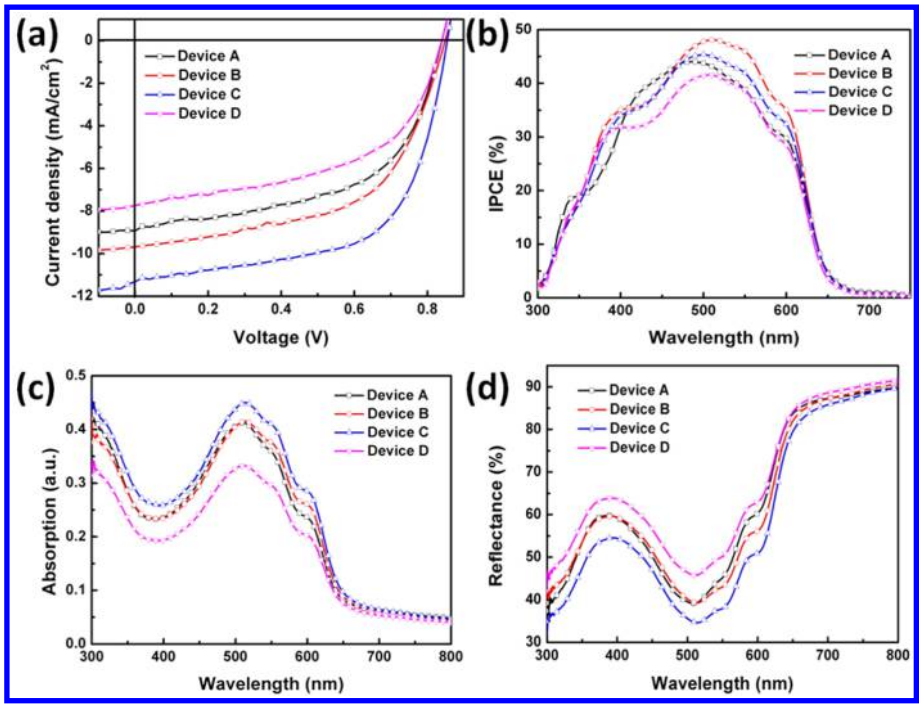

Figure 4. (a) $J-V$ characteristics of devices doped with various concentrations of CNPs, (b) IPCE spectra of all devices, (c) absorption and (d) reflection spectra of active layers without and with CNPs.

Table 1. Photovoltaic Parameters of OSCs, Including Open-Circuit Voltage (V_{oc}), Short-Circuit Current Density (J_{sc}), Fill Factor (FF), Power Conversion Efficiency (PCE), Series Resistance (R_s), and Shunt Resistance (R_{sh}) Based on Different Doping Concentrations of CNPs

Device	V_{oc} (V)	J_{sc} (mA cm^{-2})	FF (%)	PCE (%)	R_s (ohm)	R_{sh} (ohm)
A	0.84 ± 0.01	8.93 ± 0.03	54.92 ± 0.04	4.12 ± 0.03	272.92	3430.98
B	0.85 ± 0.01	9.68 ± 0.02	56.04 ± 0.03	4.60 ± 0.04	261.03	7622.51
C	0.85 ± 0.01	11.31 ± 0.01	61.09 ± 0.02	5.90 ± 0.02	147.53	6150.61
D	0.84 ± 0.01	7.74 ± 0.02	52.34 ± 0.04	3.40 ± 0.02	176.13	2221.90

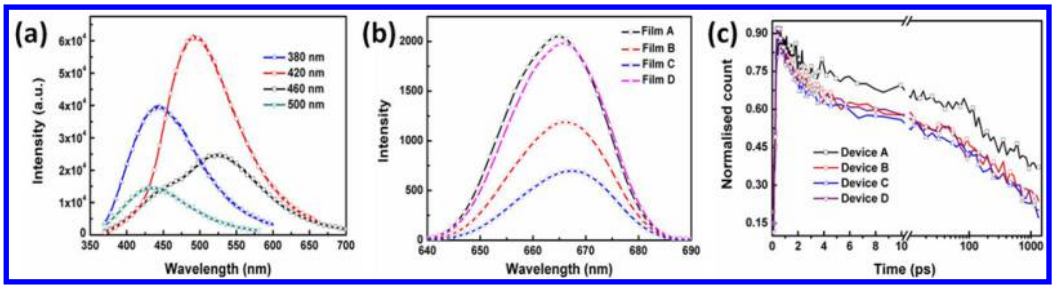

Figure 5. (a) Excitation-wavelength-dependent photoluminescence spectroscopy (PL) of the CNPs dilute aqueous solution. (b) Steady-state PL spectra of photoactive films on the top of PEI doped with different amounts of CNPs. (c) Time-resolved decay traces of pristine P3HT:ICBA and P3HT:ICBA:CNPs films with different concentration of CNPs.

(Figure 4b) of the blend films with different CNPs doping concentration.

It can be seen from Figure 5a that CNPs dilute aqueous solution exhibits excitation-wavelength-dependent photoluminescence spectroscopy (PL). Carbon nanoparticles are a kind of semiconductor, whose energy gap is related to its size. The photoluminescence spectroscopy of CNPs shows a great dependence on the excitation wavelength. The energy of excitation wavelength is closer to the energy gap, and the intensity of photoluminescence is higher. The strongest emission is observed centered at 500 nm under 420 nm excitation with PL quantum yield of 18%, indicating $\pi-\pi$ conjugated structure. Steady-state PL measurements were also performed to characterize the additional exciton generation and dissociation responsible for doping CNPs into active layer, and the results are shown in Figure 5b. Pristine P3HT:ICBA films exhibit an emission around 650 nm, which gradually decreases with the increased doping amount of CNPs; such a decrease confirms the efficient charge transfer in the P3HT:ICBA interpenetrating network. Addition of CNPs into the P3HT solutions effectively quenches the photoexcited electrons, and effectively mediates electron transfer, which benefits the mitigating of the charge, and, thus, contributes to the charge density enhancement and results in a higher photocurrent. To

DOI: 10.1021/acssuschemeng.6b00036
ACS Sustainable Chem. Eng. 2016, 4, 2359−2365

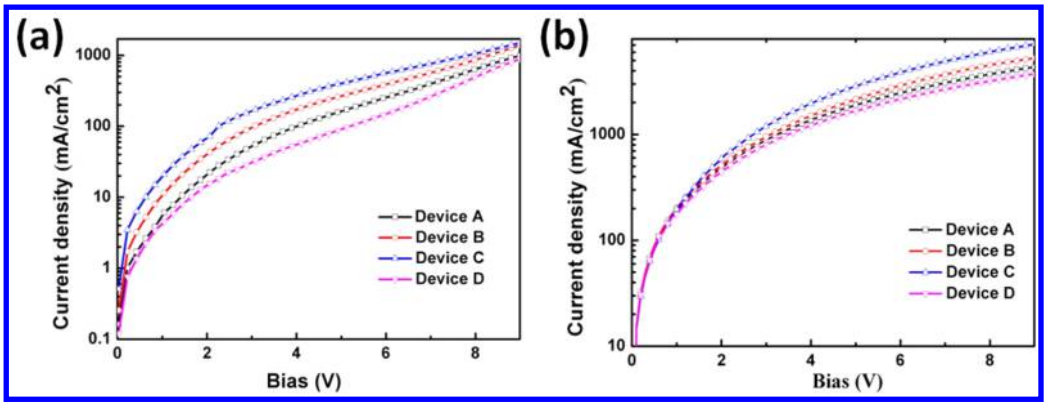

Figure 6. $J-V$ characteristics of single carrier device in dark: (a) hole-only device and (b) electron-only device.

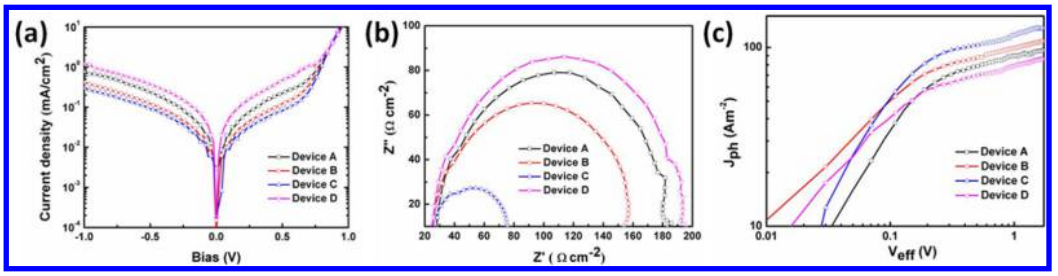

Figure 7. (a) $J-V$ characteristics of completed devices doping with different concentrations of CNPs in dark. (b) The impedance spectra diagram of all devices. (c) Plots of photocurrent density (J_{ph}) with respect to the effective voltage (V_{eff}) for control and doped devices under constant incident light intensity.

further investigate the role of CNPs in improving the performance of doped OSCs, femtosecond transient absorption (TA) spectroscopy was performed for P3HT:ICBA and P3HT:ICBA:CNPs films at 420 nm excitation. Figure 5c shows the photoexcitation signal decay in P3HT:ICBA and P3HT:ICBA:CNPs films. The doped films exhibit a faster decay than that of pristine active film, which reveals that the ultrafast photoinduced charge transfer has occurred. Additionally, the results indicate that not only do the doped cells display a larger number of initial mobile carriers than the control device, but also the carriers are extracted more rapidly. This process is beneficial for electron transfer across the whole active layer, which may be responsible for the increase of J_{sc} and FF for doped devices.

To further confirm the effect of CNPs on charge transport properties, we fabricated two kinds of single carrier devices. The hole-only device structure is ITO/MoO_3/active layer/MoO_3/Ag, and the MoO_3 is the electron blocking layer. The electron-only device structure is ITO/PEI/active layer/BCP/Ag; the BCP acts as a hole blocking layer. The $J-V$ characteristics of these two kinds of devices under the same driving voltage range from 0 to 9 V and in the absence of illumination are shown in Figure 6. Compared with control device, Device B and Device C present higher electron and hole current densities, which are in keeping with the results in Figure 4a. The current density mainly depends on the directional movement of electrons or holes under the driving bias in dark; therefore, the doped cells with suitable amounts possess better transport capacity for both electrons and holes, leading to the improvement of J_{sc}. When the doping amount of CNPs reaches 4 wt%, the performance of Device D is reduced. The heavy doping may cause more charge carrier traps and a serious charge recombination, which is a disadvantage to charge transfer. Charge carrier mobilities were calculated from space charge limited current (SCLC) model for a realistic evaluation of the enhancement of charge transfer.[48] At a typical applied voltage of 1.0 V, corresponding to an electric field of 10^5 V cm^{-1} across the bulk of a 100 nm active layer, apparent hole mobilities of 5.5×10^{-3} cm^2 V^{-1} s^{-1}, 5.7×10^{-3} cm^2 V^{-1} s^{-1}, and 5.4×10^{-3} cm^2 V^{-1} s^{-1} (Figure 6a) and electron mobilities of 2.88×10^{-4} cm^2 V^{-1} s^{-1}, 5.27×10^{-4} cm^2 V^{-1} s^{-1}, and 1.52×10^{-4} cm^2 V^{-1} s^{-1}(Figure 6b) have been determined for Device B, Device C, and Device A, respectively. With the increased doping amount of CNPs, the charge carrier mobility first enhanced and then reduced. Under an optimal doping concentration, the active layer can form efficient charge transport paths, apparent increases of charge carrier mobilities, and reduced current losses through recombination; hence, they can be efficiently swept out transporting to the electrodes, contributing to the photocurrent.

As the dark current $J-V$ characteristics of solar cells may provide useful information to estimate the performance loss and device efficiency, the dark $J-V$ characteristic of undoped and doped devices is shown in Figure 7a. Except for Device D, the doped devices display a smaller leakage current at negative voltages. The addition of CNPs into active layer can systematically ameliorate the morphology and charge transport properties, leading to an enhancement of dark J_{sc}. At a low doping concentration, the diode rectification ratios of devices are moderately improved, indicating that the devices with CNPs doping have a relatively higher conductivity, increased R_{sh}, and decreased R_s, which contribute to the improvement of FF.[47] In order to obtain information about the interfacial characteristics and internal resistance of the doped devices, electrochemical impedance spectroscopy (EIS) measurement was carried out at the frequency between 20 Hz and 1 MHz and is shown in Figure 7b. In a wide frequency range, the data are satisfactorily described by the equivalent circuit model

DOI: 10.1021/acssuschemeng.6b00036
ACS Sustainable Chem. Eng. 2016, 4, 2359−2365

containing two RC components in parallel. The smallest impedance is corresponding to the optimal doping concentration in our study, which undoubtedly helps reduce current losses across the contacting materials. The result gives a R_s of 272.92 Ω for the pristine P3HT:ICBA device, and a reduced R_s of 147.53 Ω after adding the CNPs at a concentration of 3 wt%. Since the injection barrier is decreased after doping of CNPs, the bias is mostly applied on the active layer rather than on the resistance across the contacts, resulting in an increase of J_{sc}.

We simulated the saturation current density (J_{sat}) and the maximum exciton generation rate (G_{max}) to investigate the effect of CNPs introduction on photocurrent density (J_{ph}) versus effective voltage (V_{eff}) at a double-logarithmic scale, which is shown in Figure 7c. J_{ph} is determined by the equation $J_{ph} = J_L - J_D$, where J_L and J_D are the current density measured under illumination and dark condition, respectively. The plot of J_{ph} is with respect to the effective voltage ($V_{eff} = V_0 - V$), where V_0 is the voltage at which $J_{ph} = 0$ and V is the applied bias voltage. It can be seen from Figure 7c that J_{ph} increases sharply in a linear manner at a low value of V_{eff} and then tends to saturate at a sufficiently high value of V_{eff}, and the saturated photocurrent density increases with CNPs doping. Hypothesizing that all the photogenerated excitons are dissociated into free charge carriers and collected validly at a high V_{eff}, the values of the saturation photocurrent density (J_{sat}) correlated to the maximum exciton generation rate (G_{max}), which is mainly limited by total amount of absorbed incident photons.[49,50] G_{max} could be calculated by $J_{sat} = eG_{max}L$ (L is the thickness of active layer about 100 nm).The values of G_{max} for the control and doped devices are 6.09×10^{27} m^{-3} s^{-1} (J_{sat} = 97.39 A m^{-2}), 6.88×10^{27} m^{-3} s^{-1} (J_{sat} = 110.09 A m^{-2}), 8.19×10^{27} m^{-3}s^{-1} (J_{sat} = 130.97 A m^{-2}), and 5.34×10^{27} m^{-3} s^{-1} (J_{sat} = 85.46 A m^{-2}), respectively. Thus, a noticeable enhancement in G_{max} was obtained after properly incorporating additive into the active layer, suggesting that CNPs can play an important role in the light trapping, exciton dissociation, and charge transport.

CONCLUSION

In summary, we have investigated the effects of minor doping of CNPs into the active layer on the performance of inverted OSCs based on P3HT:ICBA blending from the aspect of photoexcitation, exciton dissociation into charge carriers, and charge transport. Increasing J_{sc} and FF were observed in the devices with optimized doping concentration 3 wt%. A maximum 43.20% enhancement in power conversion efficiency (from 4.12% to 5.90%) was achieved compared with the control cell. We attribute the improvement primarily to an initial boost in charge carriers due to a perfect homogeneous interpenetrating network, which benefits charge carriers' transport and reduces charge recombination, as well as the increased absorption caused by scattering effect in the active layer induced by CNPs. Moreover, the solution processability of a CNPs doping enhances the efficiency of cells dramatically, and does not require any modification of the conventional solution processing of polymer-based organic solar cells. Doping with nanoscale additives provided a conscious and robust method to achieve further device performance enhancement, which is crucial for the potential development of low-cost, large-area printable devices.

AUTHOR INFORMATION

Corresponding Authors

* Tel: +86 431 85168241-8221. Fax: +86 431 85168270. Email: guowb@jlu.edu.cn
* Email: qusn@ciomp.ac.cn

Notes

The authors declare no competing financial interest.

ACKNOWLEDGMENTS

The authors are grateful to National Natural Science Foundation of China (61275035, 61370046, 11574110), Project of Science and Technology Development Plan of Jilin Province (20130206075SF, 20140101060JC, 20150519003JH), Scientific Frontier and Interdiscipline Innovative Projects of Jilin University (2013ZY18), Key Technology Research and Development Program of Changchun (13KG66), the Opened Fund of the State Key Laboratory on Integrated Optoelectronics (IOSKL2013KF10), and Project of Graduate Innovation Fund of Jilin University (2015098) for the support to the work.

REFERENCES

(1) Chen, X.; Jia, B. H.; Zhang, Y. A.; Gu, M. Exceeding the Limit of Plasmonic Light Trapping in Textured Screen-printed Solar Cells Using Al Nanoparticles and Wrinkle-like Graphene Sheets. *Light: Sci. Appl.* **2013**, *2*, e92.

(2) Li, X. C.; Xie, F. X.; Zhang, S. Q.; Hou, J. H.; Choy, W. C. MoO_x and V_2O_x as Hole and Electron Transport Layers Through Functionalized Intercalation in Normal and Inverted Organic Optoelectronic Devices. *Light: Sci. Appl.* **2015**, *4*, e273.

(3) Li, G.; Zhu, R.; Yang, Y. Polymer Solar Cells. *Nat. Photonics* **2012**, *6*, 153−161.

(4) Dennler, G.; Scharber, M. C.; Brabec, C. J. Polymer-fullerene Bulkheterojunction Solar Cells. *Adv. Mater.* **2009**, *21*, 1323−1338.

(5) Kim, Y.; Cook, S.; Tuladhar, S. M.; Choulis, S. A.; Nelson, J.; Durrant, J. R.; Bradley, D. D. C.; Giles, M.; Mcculloch, I.; Ha, C. S.; Ree, M. A Strong Regioregularity Effect in Self-organizing Conjugated Polymer Films and High-efficiency Polythiophene: fullerene Solar Cells. *Nat. Mater.* **2006**, *5*, 197−203.

(6) Park, B. C.; Yun, S. H.; Cho, C. Y.; Kim, Y. C.; Shin, J. C.; Jeon, H. G.; Huh, Y. H.; Hwang, I. C.; Baik, K. Y.; Lee, Y. I.; et al. Surface Plasmon Excition in Semitransparent Inverted Polymer Photovoltaic Devices and Their Applications as Label-free Optical Sensors. *Light: Sci. Appl.* **2014**, *3*, e222.

(7) Peumans, P.; Uchida, S.; Forrest, S. R. Efficient Bulk Heterojunction Photovoltaic Cells Using Small-molecular-weight Organic Thin Films. *Nature* **2003**, *425*, 158−162.

(8) Collins, B. A.; Tumbleston, J. R.; Ade, H. Miscibility, Crystallinity, and Phase Development in P3HT/PCBM Solar Cells: Toward an Enlightened Understanding of Device Morphology and Stability. *J. Phys. Chem. Lett.* **2011**, *2*, 3135−3145.

(9) He, Z. C.; Xiao, B.; Liu, F.; Wu, H. B.; Yang, Y. L.; Xiao, S.; Wang, C.; Russell, T. P.; Cao, Y. Single-junction Polymer Solar Cells With High Effiency and Photovoltage. *Nat. Photonics* **2015**, *9*, 174−179.

(10) Liu, Y. H.; Zhao, J. B.; Li, Z. K.; Mu, C.; Ma, W.; Hu, H. W.; Jiang, K.; Lin, H.; Ade, H.; Yan, H. Aggregation and Morphology Control Enables Multiple Cases of High-effiency Polymer Solar Cells. *Nat. Commun.* **2014**, *5*, 5293.

(11) Kan, B.; Li, M.; Zhang, Q.; Liu, F.; Wan, X.; Wang, Y.; Ni, W.; Long, G.; Yang, X.; Feng, H.; et al. A Series of Simple Oligomer-like Small Molecules Based on Oligothiophenes For Solution-Processed Solar Cells with High Effiency. *J. Am. Chem. Soc.* **2015**, *137*, 3886−3893.

DOI: 10.1021/acssuschemeng.6b00036
ACS Sustainable Chem. Eng. 2016, 4, 2359−2365

(12) He, Y.; Chen, H. Y.; Hou, J.; Li, Y. Indene−C_{60} Bisadduct: A New Acceptor for High-Performance Polymer Solar Cells. *J. Am. Chem. Soc.* **2010**, *132*, 1377−1382.
(13) Blom, P. W. M.; Mihailetchi, V. D.; Koster, L. J. A.; Markov, D. E. Device Physics of Polymer: Fullerene Bulk Heterojunction Solar Cells. *Adv. Mater.* **2007**, *19*, 1551−1566.
(14) Cowan, S. R.; Roy, A.; Heeger, A. J. Recombination in Polymer-fullerene Bulk Heterojunction Solar Cells. *Phys. Rev. B: Condens. Matter Mater. Phys.* **2010**, *82*, 245207.
(15) Shuttle, C. G.; O'Regan, B.; Ballantyne, A. M.; Nelson, J.; Bradley, D. D. C.; Durrant, J. R. Bimolecular Recombination Losses in Polythiophene: Fullerene Solar Cells. *Phys. Rev. B: Condens. Matter Mater. Phys.* **2008**, *78*, 113201.
(16) Kosten, E. D.; Atwater, J. H.; Parsons, J.; Polman, A.; Atwater, H. A. Highly Efficient GaAs Solar Cells by Limiting Light Eemission Angle. *Light: Sci. Appl.* **2013**, *2*, e45.
(17) Edwards, C.; Arbabi, A.; Popescu, G.; Goddard, L. L. Optically Monitoring and Controlling Nanoscale Topography During Semiconductor Etching. *Light: Sci. Appl.* **2012**, *1*, e30.
(18) Taylor, R. A.; Otanicar, T.; Rosengarten, G. Nanofluid-based Optical Filter Optimization For PV/T Systems. *Light: Sci. Appl.* **2012**, *1*, e34.
(19) Xiang, C.; Koo, W.; So, F.; Sasabe, H.; Kido, J. A Systematic Study On Efficiency Enhancements in Phosphorescent Green, Red and Blue Microcavity Organic Light Emitting Devices. *Light: Sci. Appl.* **2013**, *2*, e74.
(20) Lepage, D.; Jimenez, A.; Beauvais, J.; Dubowski, J. J. Conic Hyperspectral Dispersion Mapping Applied to Semiconductor Plasmonicss. *Light: Sci. Appl.* **2012**, *1*, e28.
(21) Xu, M. F.; Liao, Y. J.; Zu, F. S.; Liang, J.; Yuan, D. X.; Wang, Z. K.; Liao, L. S. Work-function Tuneable and Aaqueous Solution-processed Cs2CO3 for High-performance Polymer Solar Cells. *J. Mater. Chem. A* **2014**, *2*, 9400−9404.
(22) Peet, J.; Kim, J. Y.; Coates, N. E.; Ma, W. L.; Moses, D.; Heeger, A. J.; Bazan, G. C. Effiency Enhancement in Low-bandgap Polymer Solar Cells by Processing with Alkane Dithiols. *Nat. Mater.* **2007**, *6*, 497−500.
(23) Lee, K. J.; Ma, W. L.; Brabec, C. J.; Yuen, J.; Moon, J. S.; Kim, J. Y.; Lee, K.; Bazan, G. C.; Heeger, A. J. Processing Additives for Improved Effiency from Bulk Heterojunction Solar Ccells. *J. Am. Chem. Soc.* **2008**, *130*, 3619−3623.
(24) Cheng, P.; Li, Y.; Zhan, X. Effient Ternary Blend Polymer Solar Cells with Iindene-C_{60} Bisadduct as An Electron-cascade Acceptor. *Energy Environ. Sci.* **2014**, *7*, 2005−2011.
(25) Honda, S.; Nogami, T.; Ohkita, H.; Benten, H.; Ito, S. Improvement of The Light-harvesting Effiency in Polymer/fullerene Bulk Heterojunction Solar Cells by Interfacial Dye Modification. *ACS Appl. Mater. Interfaces* **2009**, *1*, 804−810.
(26) Itskos, G.; Othonos, A.; Rauch, T.; Tedde, S. F.; Hayden, O.; Kovalenko, M. V.; Heiss, W.; Choulis, S. A. Optical Properties of Organic Semiconductor Blends with Nearinfrared Quantum-dot Sensitizers for Light Harvesting Applications. *Adv. Energy Mater.* **2011**, *1*, 802−812.
(27) Lee, S. H.; Park, J. S.; Lim, B. K.; Mo, C. B.; Lee, W. J.; Lee, J. M.; Hong, S. H.; Kim, S. O. Highly Entangled Carbon Nanotube Scaffolds by Self-organized Aqueous Droplets. *Soft Matter* **2009**, *5*, 2343−2346.
(28) Dresselhaus, M. S.; Dresselhaus, G.; Avouris, P. *Carbon Nanotubes: synthesis, Structure, Properties and Applications*; Springer-Verlag: Berlin, Heidelberg, NY. 2001.
(29) Choi, H.; Ko, S.; Choi, Y.; Joo, P.; Kim, T.; Lee, B. R.; Jung, J.; Choi, H. J.; Cha, M.; Jeong, J.; Hwang, I.; Song, M. H.; Kim, B.; Kim, J. Y. Versatile Surface Plasmon Resonance of Carbon-dot-supported Silver Nanoparticles in Polymer Optoelectronic Devices. *Nat. Photonics* **2013**, *7*, 732−738.
(30) Su, Y. H.; Ke, Y. F.; Cai, S. L.; Yao, Q. Y. Surface Plasmon Resonance of Layer-by-layer Gold Nanoparticles induced Photoelectric Current in Environmentally-friendly Plasmon-sensitized Solar Cell. *Light: Sci. Appl.* **2012**, *1*, e14.
(31) Lu, L.; Luo, Z.; Xu, T.; Yu, L. Cooperative Plasmonic Effct of Ag and Au Nanoparticles on Enhancing Performance of Polymer Solar Cells. *Nano Lett.* **2013**, *13*, 59−64.
(32) Huang, J. S.; Goh, T.; Li, X. K.; Sfeir, M. Y.; Bielinski, E. A.; Tomasulo, S.; Lee, M. L.; Hazari, N.; Taylor, A. D. Polymer Bulk Heterojunction Solar Cells Employing Forster Resonance Energy Transfer. *Nat. Photonics* **2013**, *7*, 479−485.
(33) Xu, M. F.; Zhu, X. Z.; Shi, X. B.; Liang, J.; Jin, Y.; Wang, Z. K.; Liao, L. S. Plasmon Resonance Enhanced Optical Absorption in Inverted Polymer/Fullerene Solar Cells with Metal Nanoparticle-Doped Solution-Processable TiO2 Layer. *ACS Appl. Mater. Interfaces* **2013**, *5*, 2935−2942.
(34) Lou, Y. H.; Wang, Z. K.; Yuan, D. X.; Okada, H.; Liao, L. S. Interfacial Degradation Effects of Aqueous Solution-processed Molybdenum Ttrioxides on the Stability of Organic Solar Cells Evaluated by a Differential Method. *Appl. Phys. Lett.* **2014**, *105*, 113301.
(35) Lee, K. S.; Lee, J. A.; Mazor, B. A.; Forrest, S. R. Transforming the Cost of Solar-to-Electrical Energy Conversion: Integrating Thin-film GaAs Solar Cells with Non-tracking Mini-Concentrators. *Light: Sci. Appl.* **2015**, *4*, e288.
(36) Qu, S.; Liu, X.; Guo, X.; Chu, M.; Zhang, L.; Shen, D. Amplified Spontaneous Green Emission and Lasing Emission from Carbon Nanoparticles. *Adv. Funct. Mater.* **2014**, *24*, 2689−2695.
(37) Qu, S.; Wang, X.; Lu, Q.; Liu, X.; Wang, L. A Biocompatible Fluorescent Ink Based on Water-Soluble Luminescent Carbon Nanodots. *Angew. Chem.* **2012**, *124*, 12381−12384.
(38) Chen, W.; Nikiforov, M. P.; Darling, S. B. Morphology Characterization in Organic and Hybrid Solar Cells. *Energy Environ. Sci.* **2012**, *5*, 8045−8074.
(39) Holman, Z. C.; De Wolf, S.; Ballif, C. Improving Metal Reflectors by Suppressing Surface Plasmon Polaritors: A Priori Calculation of the Internal Reflectance of a Solar Cell. *Light: Sci. Appl.* **2013**, *2*, e106.
(40) Rogers, J. T.; Schmidt, K.; Toney, M. F.; Kramer, E. J.; Bazan, G. C. Structural Order in Bulk Heterojunction Films Prepared with Solvent Additives. *Adv. Mater.* **2011**, *23*, 2284−2288.
(41) Hoppe, H.; Sariciftci, N. S.; Mater, J. Organic Solar Cells: An Overview. *J. Mater. Res.* **2004**, *19*, 1924−1945.
(42) Liu, X.; Wen, W.; Bazan, G. C. Post-Deposition Treatment of An Arylated-carbazole Conjugated Polymer for Solar Cell Fabrication. *Adv. Mater.* **2012**, *24*, 4505−4510.
(43) Mihailetchi, V. D.; Wildeman, J.; Blom, P. W. M. Space-charge Limited Photocurrent. *Phys. Rev. Lett.* **2005**, *94*, 126602.
(44) Zhou, H.; Zhang, Y.; Seifter, J.; Collins, S. D.; Luo, C.; Bazan, G. C.; Nguyen, T. Q.; Heeger, A. J. High-efficiency Polymer Solar Cells Enhanced by Solvent Treatment. *Adv. Mater.* **2013**, *25*, 1646−1652.
(45) Yu, G.; Gao, J.; Hummelen, J. C.; Wudl, F.; Heeger, A. J. Polymer Photovoltaic Cells: Enhanced Efficiencies via A Network of Internal Donor-acceptor Heterojunctions. *Science* **1995**, *270*, 1789−1791.
(46) Roman, L. S.; Andersson, M. R.; Yohannes, T.; Inganas, O. Photodiode Performance and Nanostructure of Polythiophene/C_{60} Blends. *Adv. Mater.* **1997**, *9*, 1164−1168.
(47) Dittmer, J. J.; Marseglia, E. A.; Friend, R. H. Electron Trapping in Dye/Polymer Blend Photovoltaic Cells. *Adv. Mater.* **2000**, *12*, 1270−1274.
(48) Shuttle, C. G.; Hamilton, R.; O'Regan, C. B.; Nelson, J.; Durrant, J. R. Charge-density-based Analysis of The Current−voltage Response of Polythiophene/Fullerene Photovoltaic Devices. *Proc. Natl. Acad. Sci. U. S. A.* **2010**, *107*, 16448−16452.
(49) Goh, C.; Kline, R. J.; Mcgehee, M. D.; Kadnikova, E. N.; Frechet, J. M. J. Molecular-weight-dependent Mobilities in Regioregular Poly(3-hexyl-thiophene) Diodes. *Appl. Phys. Lett.* **2005**, *86*, 122110.
(50) Mihailetchi, V. D.; Koster, L. J. A.; Hummelen, J. C.; Blom, P. W. M. Photocurrent Generation in Polymer-fullerene Bulk Heterojunctions. *Phys. Rev. Lett.* **2004**, *93*, 216601.

DOI: 10.1021/acssuschemeng.6b00036
ACS Sustainable Chem. Eng. 2016, 4, 2359−2365